e-oxide laterally confined whispering-gallery mode laser vertical emission

1996

H. Deng, Q. Deng, and D. G. Deppe
Microelectronics Research Center, Department of Electrical and Computer Engineering, The University of Texas at Austin, Austin, Texas 78712-1084

Appl. Phys. Lett., Vol. 69, No. 21, 18 November 199

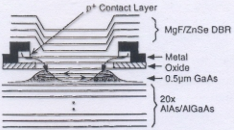

FIG. 1. Schematic of the VCSEL structure indicating the whispering-gallery mode formed in the active region.

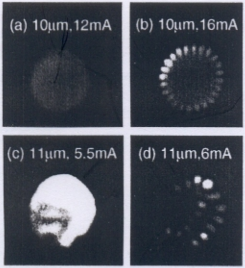

FIG. 2. Near-field radiation patterns. Top row is for a 10-μm-diam device with three MgF/ZnSe pairs at current levels of (a) 12 mA (spontaneous), (b) 16 mA (lasing). Bottom row is for an 11-μm-diam device with four MgF/ZnSe pairs at current levels of (c) 5.5 mA (spontaneous), (d) 6 mA (lasing).

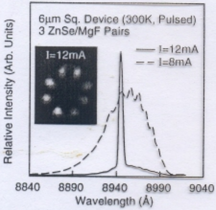

FIG. 3. Spectral data characterizing a 6-μm-diam device with three MgF/ZnSe pairs at current levels of 8 mA (spontaneous, dashed line) and 12 mA (lasing, solid line). The inset is the lasing near-field radiation pattern at a current level of 12 mA.

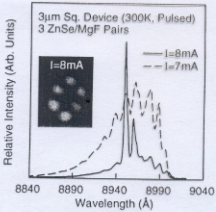

FIG. 4. Spectral data characterizing a 3-μm-diam device with three MgF/ZnSe pairs at current levels of 7 mA (spontaneous, dashed line) and 8 mA (lasing, solid line). The inset is the lasing near-field radiation pattern at a current level of 8 mA.

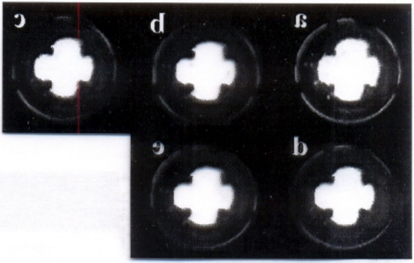

at 7 mA current injection

(a) without polariser
(b) θ = 0 ° (c) θ = 45 °
(d) θ = 90 ° (e) θ = 135 °

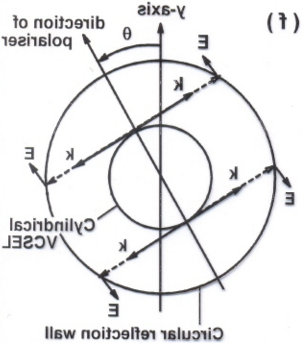

<u>Near field patterns of VCSEL device</u>

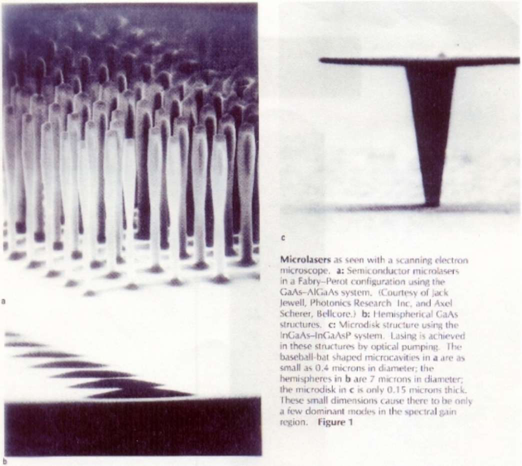

Microlasers as seen with a scanning electron microscope. **a:** Semiconductor microlasers in a Fabry–Perot configuration using the GaAs–AlGaAs system. (Courtesy of Jack Jewell, Photonics Research Inc, and Axel Scherer, Bellcore.) **b:** Hemispherical GaAs structures. **c:** Microdisk structure using the InGaAs–InGaAsP system. Lasing is achieved in these structures by optical pumping. The baseball-bat shaped microcavities in **a** are as small as 0.4 microns in diameter; the hemispheres in **b** are 7 microns in diameter; the microdisk in **c** is only 0.15 microns thick. These small dimensions cause there to be only a few dominant modes in the spectral gain region. **Figure 1**

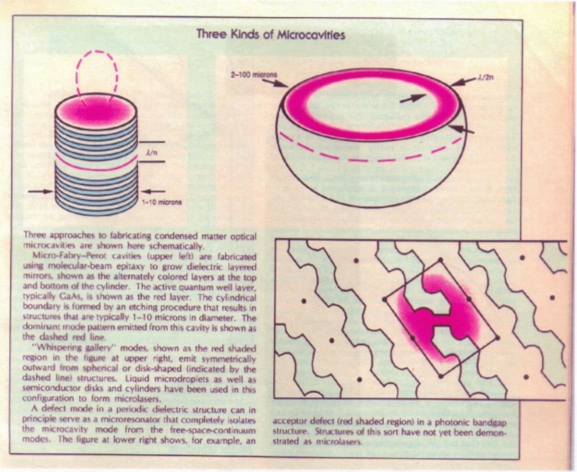

Three Kinds of Microcavities

Three approaches to fabricating condensed matter optical microcavities are shown here schematically.

Micro-Fabry–Perot cavities (upper left) are fabricated using molecular-beam epitaxy to grow dielectric layered mirrors, shown as the alternately colored layers at the top and bottom of the cylinder. The active quantum well layer, typically GaAs, is shown as the red layer. The cylindrical boundary is formed by an etching procedure that results in structures that are typically 1–10 microns in diameter. The dominant mode pattern emitted from this cavity is shown as the dashed red line.

"Whispering gallery" modes, shown as the red shaded region in the figure at upper right, emit symmetrically outward from spherical or disk-shaped (indicated by the dashed line) structures. Liquid microdroplets as well as semiconductor disks and cylinders have been used in this configuration to form microlasers.

A defect mode in a periodic dielectric structure can in principle serve as a microresonator that completely isolates the microcavity mode from the free-space-continuum modes. The figure at lower right shows, for example, an acceptor defect (red shaded region) in a photonic bandgap structure. Structures of this sort have not yet been demonstrated as microlasers.

$$N_2[B_{21}\rho(\nu) + A_{21}] = N_1 B_{12}\rho(\nu)$$

and, substituting for $\rho(\nu)$ from (5.2-4),

$$N_2\left[B_{21}\frac{8\pi n^3 h\nu^3}{c^3(e^{h\nu/kT}-1)} + A_{21}\right] = N_1\left[B_{12}\frac{8\pi n^3 h\nu^3}{c^3(e^{h\nu/kT}-1)}\right] \tag{5.2-6}$$

Since the atoms are in thermal equilibrium, the ratio N_2/N_1 is given by the Boltzmann factor [5] as

$$\frac{N_2}{N_1} = e^{-h\nu/kT} \tag{5.2-7}$$

Equating (N_2/N_1) as given by (5.2-6) to (5.2-7) gives

$$\frac{8\pi n^3 h\nu^3}{c^3(e^{h\nu/kT}-1)} = \frac{A_{21}}{B_{12}e^{h\nu/kT} - B_{21}} \tag{5.2-8}$$

The last equality can be satisfied only when

$$B_{12} = B_{21} \tag{5.2-9}$$

and simultaneously

$$\frac{A_{21}}{B_{21}} = \frac{8\pi n^3 h\nu^3}{c^3} \tag{5.2-10}$$

The last two equations were first given by Einstein [6]. We can, using (5.2-10), rewrite the induced transition rate (5.2-1) as

$$W_i' = \frac{A_{21}c^3}{8\pi n^3 h\nu^3}\rho(\nu) = \frac{c^3}{8\pi n^3 h\nu^3 t_{\text{spont}}}\rho(\nu) \tag{5.2-11}$$

where, because of (5.2-9) the distinction between $2 \rightarrow 1$ and $1 \rightarrow 2$ induced transition rates is superfluous.

Equation (5.2-11)

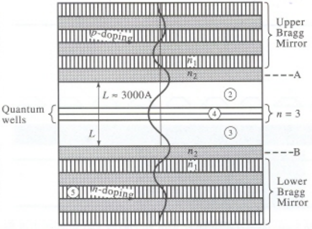

Figure 16-14 The field distribution of the laser mode inside a vertical cavity laser with $L \approx \lambda/n$ with three quantum wells. Notice the evanescent decay of the field envelope inside the Bragg mirrors and the constant amplitude standing wave between the mirrors.

total length of the spacer region, 2 and 3, that straddles the active region is typically $L = \lambda$, where λ is the wavelength in the medium. This translates, near $\lambda = 1\ \mu\text{m}$, to $L \approx 0.3\ \mu\text{m}$. Typical mode diameters are in the range of 3 to 10 μm. A typical Bragg stack consisting of, say, 15 $\lambda/4$ layers is 2 μm thick.

The field distribution inside a vertical cavity laser is shown in Figure 16-14. We note that inside the Bragg mirror the optical wave amplitude undergoes exponential evanescence. This is in agreement with Equation (13.5-4) and Figures 13-7 and 18-8, which describe the evanescent decay of an optical wave inside a periodic medium for optical frequencies within the "forbidden" frequency gap [17].

Since the distance L_z traveled in the amplifying medium is small (approximately 100 Å per quantum well), the gain per pass is very small, and laser oscillation is made possible by the extremely high reflectance (>99 percent) of the Bragg mirror and the very low losses in regions 2 and 3. Figure 16-14 conveys the relative scale of the key layer thicknesses.

The Oscillation Condition of a Vertical Cavity Laser

The oscillation condition of the VCSEL can be written as

$$r_1(\omega)r_2(\omega)\exp\left[2\sum_{m=1}^{N}\gamma_m(\omega)L_z - i2\frac{\omega}{c}nL\right] = 1 \qquad (16.4\text{-}1)$$

which is a statement of the requirement that after one round trip a wave returns to its, arbitrary, starting plane with the same amplitude and, to within an integral multiple of 2π, the same phase. The factor of 2 in the exponent accounts for the fact that the quantum wells are placed at the peak of the standing wave pattern where they are exposed to an intensity that is twice the spatially averaged value. The number of quantum wells is N. In what follows, we will assume that each quantum well contributes equally to the gain so that $\sum_{m=1}^{N} \gamma_m(\omega)L_z \equiv N\gamma(\omega)L_z$. The average index of refraction of the path is n. The Bragg mirrors' (amplitude) reflectances $r_1(\omega)$ and $r_2(\omega)$ refer to their respective input planes A and B in Figure 16-14.

The amplitude condition of (16.4-1) is

$$|r(\omega)|^2 = \exp(-2N\gamma(\omega)L_z) \tag{16.4-2}$$

Since the optical wave travels at right angles to the plane of the quantum wells, the gain γ is not the modal gain g_{model} of (16.2-13) but the bulk gain γ of a quantum well medium. We note that according to (16.2-9), the product $\gamma(\omega)L_z$ is independent of L_z. (This is strictly true when L_z is sufficiently small so that contributions to the gain from excited states ($\ell > 1$) in the quantum well are negligible. In practice, this is satisfied at room temperature for $L_z < 70\text{Å}$.) From experimental data of edge-emitting quantum well lasers, we determine that for $L_z \approx 70$ Å the maximum gain due to the $\ell = 1$ quantized well level with a fully inverted population is $\gamma(\omega_0) \cong 5 \times 10^3\ \text{cm}^{-1}$. Using this value in (16.4-2), taking $L_z = 70\text{Å}$, leads to

$$|r(\omega)|^2 = \exp[-2N \times 5 \times 10^3 \times 7 \times 10^{-7}]$$

for the reflectivity needed for oscillation.

$$N = 1,\ |r(\omega)|^2 = 0.993$$

$$N = 2,\ |r(\omega)|^2 = 0.986$$

$$N = 3,\ |r(\omega)|^2 = 0.979$$

$$N = 4,\ |r(\omega)|^2 = 0.972$$

where N is the number of quantum wells so that reflectivities around $R(\equiv |r(\omega)|^2) = 98$ percent are required of the Bragg reflectors. We will next make a small detour to study these reflectors.

The Bragg Mirror

The analysis of the Bragg mirror is an excellent example of the power of the coupled-mode formalism developed in Chapter 13. The periodic perturbation of the index of refraction couples, exactly as in the case of the DFB laser, two waves propagating in opposite directions. The coupling is strongest when the propagation constants $\pm\beta$ of the two coupled waves

$$\begin{aligned} &B(z)\mathscr{E}_y(x, y)\exp[i(\omega t - \beta z)] \quad \text{(forward wave)} \\ &A(z)\mathscr{E}_y(x, y)\exp[i(\omega t + \beta z)] \quad \text{(backward wave)} \end{aligned} \tag{16.4-3}$$

obey very nearly the Bragg condition

$$\beta = \ell \frac{\pi}{\Lambda} \qquad \ell = 1, 2, \ldots \tag{16.4-4}$$

for some integer ℓ. If we retain in Equation (13.4-3) only the two Bragg-coupled waves $A_s^{(-)} \rightarrow A$, $A_s^{(+)} \rightarrow B$, we obtain

$$\frac{dA}{dz} = \frac{i\omega\epsilon_0}{4} B \exp(-i2\beta z) \int_{-\infty}^{\infty} \Delta n^2(x, y, z) \mathscr{E}_y^2(x, y)\, dxdy \tag{16.4-5}$$

We also assume that the modes A and B are both y-polarized and have a normalized transverse distribution, $\mathscr{E}_y(x, y)$. The index of refraction of the Bragg mirror can be represented by

$$n^2(x, y, z) = \frac{1}{2}(n_1^2 + n_2^2) + \frac{1}{2}(n_1^2 - n_2^2)\, f(z)$$

where n_1, n_2 are the indices of refraction of the two alternating layers, and $f(z)$ is a square wave of unity amplitude as shown in Figure 16-14.

$$f(z) = \sum_{\ell} a_\ell e^{i\ell\frac{2\pi}{\Lambda}z},\ a_\ell = i\frac{(e^{-i\pi\ell} - 1)}{\ell\pi}$$

$$\Delta n^2(x, y, z) = \left(\frac{n_1^2 - n_2^2}{2}\right) f(z) \tag{16.4-6}$$

Assuming that the Bragg condition (16.4-4) is satisfied by the ℓth term in the Fourier series expansion of $f(z)$, we can rewrite (16.4-5) as

$$\frac{dA}{dz} = \frac{i\omega\epsilon_0(n_1^2 - n_2^2)a_\ell}{8} \int_{-\infty}^{\infty} \mathscr{E}^2(x, y)\, dx\, dy\, B \exp\left[i\left(\ell\frac{2\pi}{\Lambda} - 2\beta\right)z\right] \tag{16.4-7}$$

when $\ell = 1$ we have

$$\frac{dA}{dz} = \kappa B \exp(i\Delta\beta z)$$

$$\frac{dB}{dz} = \kappa A \exp(-i\Delta\beta z) \tag{16.4-8}$$

$$\kappa = \frac{\omega\epsilon_0}{4\pi}(n_1^2 - n_2^2) \int_{-\infty}^{\infty} \mathscr{E}_y^2(x, y)\, dx\, dy \approx \frac{2\Delta n}{\lambda}$$

$$\Delta\beta(\omega) = 2\left(\frac{\pi}{\Lambda} - \beta(\omega)\right) \tag{16.4-9}$$

In the second approximate equality of (16.4-9), we assumed $|\Delta n| = |n_1 - n_2| \ll n_1$, n_2, $\beta \approx \omega\sqrt{\mu\epsilon_0}n$, $n^2 \equiv (1/2)(n_1^2 + n_2^2)$, and used the normalization integral, (13.2-8). Equations (16.4-8) constitute a pair of first-order, linear-coupled differential equations. Their solution requires that we specify two boundary conditions. Our chief interest is in the operation of the Bragg stack as a reflector. The incident amplitude $B(0)$ thus becomes one of the given conditions. Since the backward-going wave A is due completely to internal reflections, we take $A(L) = 0$. The solution is thus given by Equations (13.5-2) so that the amplitude reflectance is

$$r(\omega) = \frac{A(0)}{B(0)} = \frac{-i\kappa \sinh (SL)}{-\Delta\beta(\omega) \sinh (SL) + iS \cosh (SL)} \qquad (16.4\text{-}10)$$

$$S(\omega) = \sqrt{\kappa^2 - \Delta\beta(\omega)^2}$$

where $\omega_0 = \pi c/\Lambda n$ is the Bragg frequency.

To obtain an appreciation for the magnitude of reflectivities that we may expect in a typical Bragg mirror, we will design a Bragg mirror to operate at a center wavelength of $\lambda_0 = 0.875\ \mu\text{m}$. The unit cell consists of a pair of epitaxially grown $\text{Ga}_{0.8}\text{Al}_{0.2}\text{As}$ and AlAs layers. The index of refraction difference is as $\Delta n = n_{\text{Ga}_{0.8}\text{Al}_{0.2}\text{As}} - n_{\text{AlAs}} = 0.55$. The average index is $n = 3.3$. The peak reflectivity is obtained from (16.4-10) with $\Delta\beta = 0$. Since the thickness of a unit cell is $\lambda_0/2n$, the length of the Bragg mirror with N_m periods is $L = N_m\lambda_0/2n$. The result in the case of $N_m = 15$ is $R(\omega_0) = |r(\omega_0)|^2 = \tanh^2\left(N_m \frac{\Delta n}{n}\right) = \tanh^2\left(\frac{15 \times 0.55}{3.3}\right) = 0.973$. This value is sufficient, according to the discussion following (16.4-2), to satisfy the oscillation conditions in vertical cavity lasers with more than four inverted ($N \geq 4$) quantum wells.

A plot of the reflectivity $|r(\omega)|^2$ based on (16.4-10) and the experimental parameters of the above example is shown in Figure 16-15(a). An experimental plot of a Bragg mirror with the same parameters is shown in Fig. 16-15(b). The phase shift $\phi(\omega)$ of the complex reflectance $r(\omega) = |r(\omega)| \exp(-i\phi(\omega))$ is shown in Fig. 16-15(c). For a more detailed treatment of Bragg mirrors and light propagation in stratified media, the reader is referred to Reference [17].

The Oscillation Frequencies

The phase part of (16.4-1) is used to obtain an expression for the oscillation frequencies of a surface-emitting Bragg mirror laser. If, for simplicity's sake, we take two identical $r_1(\omega) = r_2(\omega) = |r(\omega)|e^{-i\phi(\omega)}$, the phase condition is

$$-\phi(\omega) + \frac{\omega}{c} nL = m\pi \qquad (16.4\text{-}11)$$

$$m = 1, 2, \ldots$$

Let us denote the two neighboring oscillation frequencies corresponding to m and $m+1$ as ω_m and ω_{m+1}, respectively:

$$-\phi(\omega_m) + \frac{\omega_m}{c} nL = m\pi$$

$$-\phi(\omega_{m+1}) + \frac{\omega_{m+1}}{c} nL = (m + 1)\pi \qquad (16.4\text{-}12)$$

so that

$$\left[-\phi(\omega_{m+1}) + \phi(\omega_m) + \frac{\omega_{m+1} - \omega_m}{c} nL\right] = \pi \qquad (16.4\text{-}13)$$

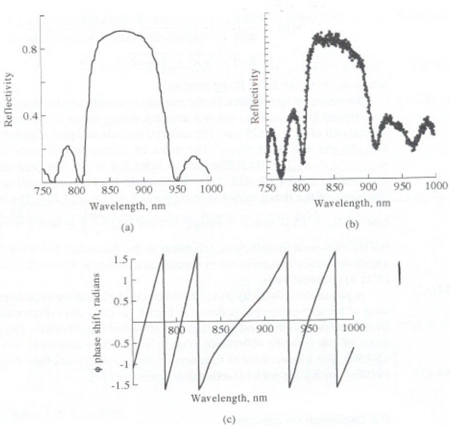

Figure 16-15 Calculated (a) and measured (b) reflectivity of a 15-period $Al_{0.2}GA_{0.8}AS/AlAs$ distributed Bragg reflector. The calculated phase shift $\phi(\omega)$ is plotted in (c). (Courtesy of J. Obrien, Caltech.)

According to Figure 16-15(c), we can approximate $\phi(\omega)$ in the region of high reflectivity by

$$\phi(\omega) \cong -a(\omega - \omega_0)$$

$$a \approx \frac{\pi n}{2\kappa c} \tag{16.4-14}$$

The expression for the slope a is obtained by dividing the maximum phase deviation of π in Figure 16-15(c) by the corresponding (horizontal) frequency interval that, according to Equation (13.5-7), is $(\Delta\omega)_{\text{gap}} = 2\kappa c/n$.

which when applied to (16.4-13) results in

$$2\pi\Delta\nu = (\omega_{m+1} - \omega_m) = \frac{\pi c}{n\left(L + \dfrac{\pi}{2\kappa}\right)} \tag{16.4-15}$$

for the intermode frequency interval.

The effective length of the Bragg mirror resonator is thus not the mirror spacing L but

$$L_{\text{eff}} = L + \frac{\pi}{2\kappa} \tag{16.4-16}$$

The contribution $\pi/2\kappa$ is due to the evanescent penetration of the oscillating laser field into the Bragg mirrors, as illustrated in Figure 16-14. Since two Bragg mirrors are assumed in the analysis, the Bragg penetration distance into a single mirror is $\pi/4\kappa$.

We recall that the field behavior inside the periodic Bragg mirror (at the Bragg frequency ω_0) is given by (13.5-6) as

$$\exp(-i\beta' z) = \exp\left(-i\frac{\pi}{\Lambda}z\right)\exp(-\kappa z)$$

which corresponds to an effective penetration distance of $\sim\kappa^{-1}$ to be compared to the value of $\pi/4\kappa$ of (16.4-16)

Numerical example—intermode frequency separation. To obtain an appreciation for the intermode frequency spacing of (16.4-15), we will consider the laser depicted in Figure 16-14. The data for the Bragg mirror is the same as used in the example following (16.4-10). The basic parameters are:

$$\lambda = 1\ \mu\text{m} \qquad L = \lambda = 1\ \mu\text{m}$$

$$\kappa = \frac{2\Delta n}{\lambda} = \frac{2 \times 0.55}{1} = 1.1\ \mu\text{m}^{-1}$$

$$L_{\text{eff}} = L + \frac{\pi}{2\kappa} = (1 + 1.427)\ \mu\text{m} = 2.427\ \mu\text{m}$$

(Note that the penetration depth, 1.427 μm, is larger than the intermirror spacing, L.)

$$\Delta\nu \equiv \frac{\omega_{m+1} - \omega_m}{2\pi} = \frac{c}{2nL_{\text{eff}}} = \frac{3 \times 10^{10}}{2 \times 3.3 \times 2.427 \times 10^{-4}}$$

$$= 1.873 \times 10^{13}\ \text{Hz} = 624.3\ \text{cm}^{-1}$$

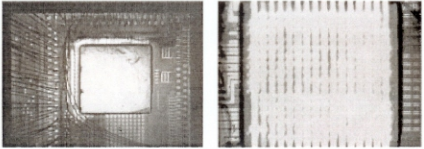

그림 1.4.1. 16 X 16 VCSEL-CMOS smart pixel 과 그 발진 모습

이 VCSEL 어레이 소자는 대부분 발진 되었지만, 열화 문제로 인하여 병렬 작동하에서는 불과 80 개만이 1 GHz 의 광변조 특성을 가지는 것으로 나타났다. 즉, 비교적 높은 mA 급 동작 전류에서 작동하는 VCSEL 소자는 어레이로 집적하여 구동할 때 수반되는 온도 상승으로 소자의 열화 문제가 등장하며, 어레이 칩 위에서 VCSEL 소자들 위치에 따른 온도 변화가 상이하므로 그 발진 파장 천이 문제들이 발생하여 광변조 특성에 문제가 발생하는 것이다. 변덕스러운 선형 편광 특성 및 TEM 횡모드를 쉽사리 제어할 수 없는 문제점도 있다. 특히, 고집적 VCSEL 어레이의 열화 문제는 실용화 이전에 반드시 풀어야 할 문제이다. 이러한 열화 문제는 소자의 turn-on 에도 영향을 주어 Fully addressable 한 특성을 망가뜨려서 칩 사용 자체가 불가능하게 만든다.

allowing the same device to be integrated as both sources and sinks. An electromagnetic simulation of this structure, shown in Figure 6, achieved optical power coupling efficiency greater than 50%. These results have encouraged efforts towards fabrication and demonstration of the PENCEL concept.

Summary/Conclusions:

This article discussed concepts for integrating optics with future deep sub-micron integrated circuits to overcome the inherent limitations of metal global wires for intra-chip communication. Analysis of global interconnection topology led to concepts for interconnection fabrics tailored to specific global communi-

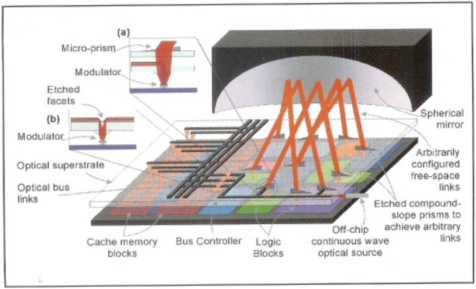

Figure 4: Notional depiction of the application-specific interconnection fabric (ASIF) concept. Inset: PENCEL configurations for (a) free-space and (b) guided wave optical fabric.

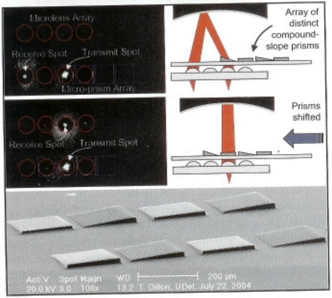

Figure 5: Links demonstrated with fabricated Silicon micro-prisms.

HEBS glass," J. of Microlitography, Microfabrication, & Micromachining, Sept. 2004.

[8] M. Iqbal, T. Dillon, M. J. McFadden, D. W. Prather, M. W. Haney, "Novel structures for optical sources based on quantum well modulators for intrachip global communication," Proc. of OSA 88th Annual Meeting: Frontiers in Optics/Laser Science, Rochester, NY, Oct. 2004.

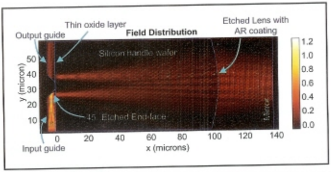

Figure 6: Finite-difference time-domain (FDTD) simulation of PENCEL concept.

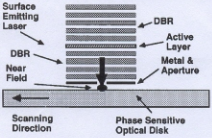

Fig. 17. VCSEL for the generation of optical near field using nano-aperture.

Vertical optical interconnects of LSI chips and circuit boards and multiple fiber systems may be the most interesting field related to VCSELs. From this point of view, the device should be as small as possible. The future process technology for it, including epitaxy and etching, will drastically change the situation of VCSELs. Some optical technologies are already introduced in various subsystems and, in addition, the arrayed microoptic technology would be very helpful for advanced systems.

The most promising application will be gigabit LANs. GaAs VCSELs emitting 850 nm of standardized wavelength are mass produced for >1–Gb/s LAN and simple optical links. For high-end systems, 1300–1550-nm devices are requested. By using VCSEL and micromachining technology, we demonstrated a temperature-insensitive surface normal Fabry–Perot filter for add–drop filtering in WDM. To establish an appropriate module technology utilizing VCSELs, an MOB has been investigated together with planar microlens array. Related to planar microlens array application and ultra-parallel information processing, an image recognition system is investigated using synthetic discriminant function (SDF) filtering.

In summary, the ultra-parallel optoelectronics based upon arrayed devices, including VCSELs, will open up a new era for the 2000 millennium.

ACKNOWLEDGMENT

The author would like to thank Prof. F. Koyama, T. Miyamoto, and other laboratory members for their collaboration and assistance in preparing the original drawings.

REFERENCES

[1] K. Iga, F. Koyama, and S. Kinoshita, "Surface emitting semiconductor laser," *IEEE J. Quant. Electron.*, vol. 24, pp. 1845–1855, Sept. 1988.

[2] K. Iga, "Surface emitting laser," *Trans. IEICE, C-I*, vol. JBI-C-1, no. 9, pp. 483–493, Sept. 1998.

[3] H. Soda, K. Iga, C. Kitahara, and Y. Suematsu, "GaInAsP/InP surface emitting injection lasers," *Jpn. J. Appl. Phys.*, vol. 18, pp. 2329–2330, Dec. 1979.

[4] K. Iga, S. Kinoshita, and F. Koyama, "Microcavity GaAlAs/GaAs surface-emitting laser with $I_{th} = 6$ mA," *Electron. Lett.*, vol. 23, no. 3, pp. 134–136, Jan. 1987.

[5] F. Koyama, S. Kinoshita, and K. Iga, "Room-temperature continuous wave lasing characteristics of GaAs vertical cavity surface-emitting laser," *Appl. Phys. Lett.*, vol. 55, no. 3, pp. 221–222, July 1989.

[6] J. L. Jewell, S. L. McCall, A. Scherer, H. H. Houh, N. A. Whitaker, A. C. Gossard, and J. H. English, "Transverse modes, waveguide dispersion and 30-ps recovery in submicron GaAs/AlAs microresonators," *Appl. Phys. Lett.*, vol. 55, pp. 22–24, July 1989.

[7] R. Geels and L. A. Coldren, "Narrow-linewidth, low threshold vertical-cavity surface-emitting lasers," in *12th IEEE Int. Semiconductor Laser Conf.*, vol. B-1, 1990, pp. 16–17.

[8] T. Wipiejewski, K. Panzlaf, E. Zeeb, and K. J. Ebeling, "Submilliamp vertical cavity laser diode structure with 2.2-nm continuous tuning," in *18th European Conf. Opt. Comm. '92*, Sept. 1992, PDII-4.

[9] Y. H. Lee, B. Tell, K. F. Brown-Goebeler, R. E. Leibenguth, and V. D. Mattera, "Deep-red continuous wave top-surface-emitting vertical-cavity AlGaAs superlattice lasers," *IEEE Photon. Technol. Lett.*, vol. 3, no. 2, pp. 108–109, Feb. 1991.

[10] T. Miyamoto, T. Uchida, N. Yokouchi, Y. Inaba, F. Koyama, and K. Iga, "A study on gain-resonance matching of CBE grown $l = 1.5$ μm surface emitting lasers," *IEEE/LEOS Annu.*, no. DLTA13.2, p. 542, Nov. 1992.

[11] T. Baba, Y. Yogo, K. Suzuki, F. Koyama, and K. Iga, "Near room temperature continuous wave lasing characteristics of GaInAsP/InP surface emitting laser," *Electron. Lett.*, vol. 29, no. 10, pp. 913–914, May 1993.

[12] D. I. Babic, K. Streubel, R. P. Mirin, J. Pirek, N. M. Margalit, J. E. Bowers, E. L. Hu, D. E. Mars, L. Yang, and K. Carey, "Room temperature performance of double-fused 1.54 μm vertical-cavity lasers," in *IPRM 96*, Apr. 1996, no. ThA1-2.

[13] K. D. Choquette, R. P. Schneider, M. H. Crawford, K. M. Geib, and J. J. Figiel, "Continuous wave operation of 640–660 nm selectively oxidised AlGaInP vertical cavity lasers," *Electron. Lett.*, vol. 31, pp. 1145–1146, July 1995.

[14] K. Iga, "Possibility of Green/Blue/UV surface emitting lasers," in *Int. Symp. Blue Laser Light Emitting Diodes*, Mar. 1996, Th-11, pp. 263–266.

[15] T. Someya, K. Tachibana, Y. Arakawa, J. Lee, and T. Kamiya, "Lasing oscillation in InGaN vertical cavity surface emitting lasers," in *16th Int. Semiconductor Laser Conf.*, 1998, PD-1, pp. 1–2.

[16] S. Uchiyama, N. Yokouchi, and T. Ninomiya, "Room-temperature CW operation of 1.3-μm GaInAsP SL-MQW surface emitting laser," in *43th Spring Meeting Jpn. Soc. Appl. Phys.*, 1996, 26p-C-7.

[17] N. M. Margalit, D. I. Babic, K. Streubel, R. P. Mirin, R. L. Naone, J. E. Bowers, and E. L. Hu, "Submilliamp long wavelength vertical cavity lasers," *Electron. Lett.*, vol. 32, p. 1675, Aug. 1996.

[18] K. A. Black, N. M. Margalit, E. R. Hegblom, P. Abraham, Y.-J. Chiu, J. Piprek, J. E. Bowers, and E. L. Hu, "Double-fused 1.5 μm vertical cavity lasers operating continuous wave up to 71 °C," in *16th Int. Semiconductor Laser Conf.*, 1998, ThA8, pp. 247–248.

[19] V. Jayaraman, J. C. Geske, M. H. MacDougal, F. H. Peters, T. D. Lowes, and T. T. Char, "Uniform threshold current, continuous-wave, single mode 1300 nm vertical cavity lasers from 0 to 70 °C," *Electron. Lett.*, vol. 34, no. 14, pp. 1405–1407, July 1998.

[20] M. Yamada, T. Anan, K. Kurihara, K. Nishi, K. Tokutome, A. Kamei, and S. Sugou, "Room temperature low threshold CW operation of 1.23 μm GaAsSb VCSELs of GaAs substrates," *Electron. Lett.*, vol. 36, no. 7, pp. 637–638, Mar. 2000.

[21] E. Hall, G. Almuneau, J. K. Kim, O. Sjölund, H. Kroemer, and L. A. Coldren, "Electrically-pumped, single-epitaxial VCSELs at 1.55 μm with Sb-based mirrors," *Electron. Lett.*, vol. 35, no. 16, pp. 1337–1338, Aug. 1999.

[22] S. Sekiguchi, T. Miyamoto, T. Kimura, F. Koyama, and K. Iga, "Self-arraigned current confinement structure using AlAs/InP tunnel junction in GaInAsP/InP semiconductor lasers," *Appl. Phys. Lett.*, vol. 75, no. 11, pp. 1512–1514, Sep. 1999.

[23] C. Kazmierski, J. P. Debray, R. Madani, N. Bouadma, J. Etrillard, I. Sagnes, F. Alexandre, and M. Quillec, "First all-monolithic VCSELs on InP: +55 °C pulse lasing at 1.56 μm with GaInAlAs/InP system," in *16th Int. Semiconductor Laser Conf.*, 1998, PD-3, pp. 5–6.

[24] M. Kondow, K. Nakahara, T. Kitatani, Y. Yazawa, and K. Uomi, "GaInNAs laser diode pulsed operation at 77 K," in *OECC'96*, 18D-3-2.

[25] K. Nakahara, M. Kondow, T. Kitatani, M. C. Larson, and K. Uomi, "1.3-μm continuous-wave lasing operation in GaInNAs quantum-well lasers," *IEEE Photon. Technol. Lett.*, vol. 10, pp. 487–488, Apr. 1998.

[26] K. Iga, "Vertical cavity surface emitting lasers based on InP and related compounds—Bottleneck and corkscrew," in *Conf. Indium Phosphide Related Materials*, Schwabisch Gmund, Germany, Apr. 1996.

[27] T. Miyamoto, K. Takeuchi, F. Koyama, and K. Iga, "Novel GaInNAs/GaAs quantum well structure for long wavelength semiconductor lasers," *IEEE Photon. Technol. Lett.*, vol. 9, pp. 1448–1450, Nov. 1997.

[28] M. C. Larson, M. Kondow, T. Kitatani, K. Nakahara, K. Tamura, H. Inoue, and K. Uomi, "Room-temperature pulsed operation of GaInNAs/GaAs long-wavelength vertical cavity lasers," in *IEEE/LEOS'97*, Nov. 1997, no. PD1.3.

[29] T. Kageyama, T. Miyamoto, S. Makino, N. Nishiyama, F. Koyama, and K. Iga, "High-temperature operation up to 170 °C of GaInNAs–GaAs quantum-well lasers grown by chemical beam epitaxy," *IEEE Photon. Technol. Lett.*, vol. 12, pp. 10–12, Jan. 2000.

March 1990
Volume 29 Number 3
ISSN 0091-3286

The International
Society for
Optical Engineering

Optical Engineering

Photonic Switching & Interconnects

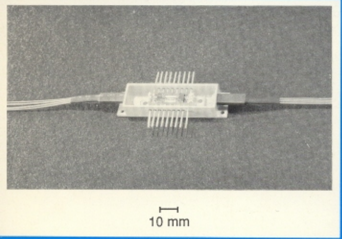

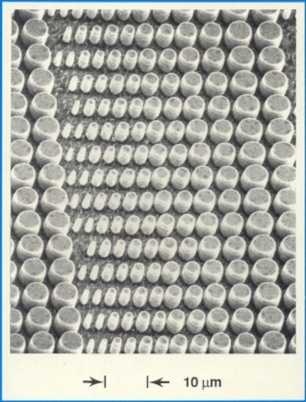

o in this issue:

er Scanners

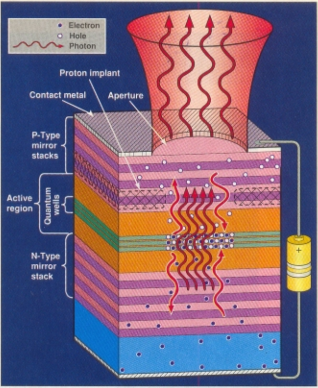

Sandia National Laboratories

The mirrors of a vertical-cavity surface-emitting laser are paired layers of semiconductor materials, which together reflect more than 99 percent of photons at the lasing wavelength. The active region sandwiched between the mirrors includes several quantum wells—ultrathin layers that trap electrons [dots] and holes [open circles] injected from metal contacts applied to the substrate and top mirror. In the quantum wells the carriers recombine to produce photons [wavy arrows]. Photons of the right wavelength multiply as they bounce between the mirrors. Some of the photons leak out of the top mirror through an aperture defined in the top metal contact to produce an intense beam of coherent light.

for vertical cavity lasers

active volume makes the required threshold current extremely small (<40 µA).[4,5]

The oxide aperture in the VCSEL can be fabricated with extremely small dimensions, small enough that the optical modes of the device begin to become confined in all three dimensions to distances of the order of the emitted wavelength. For lasers this small, the standard approximations used to predict the operation of the device begin to break down. To further improve the device characteristics, we are undertaking the study of ultra-small devices in order to develop accurate models for predicting device performance.[6]

It is not hard to imagine that controlling the oxidation reaction with sufficient precision to form devices with sub-micron features is quite difficult. The oxidation reaction is typically conducted in a quartz tube zone furnace, with a nitrogen-fed water bubbler supplying the necessary vapor. With this configuration, monitoring of the sample during the oxidation is difficult if not impossible. Great effort must be expended, therefore, to ensure that the oxidation conditions are repeatable and stable so that timed oxidations produce the desired features. In order to facili-

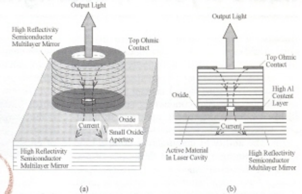

Figure 1. (a) Perspective illustration of a typical VCSEL. (b) Cross-sectional illustration of the same structure.

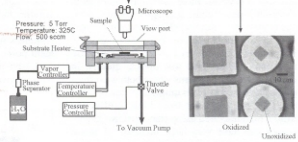

Figure 2. Schematic diagram of the oxidation furnace, with an infrared photograph of a device undergoing oxidation.